Nuclear breathing mode in neutron-rich nickel isotopes: Sensitivity to the symmetry energy and the role of the continuum

J. Piekarewicz

Phys. Rev. C **91**, 014303 — Published 5 January 2015

DOI: 10.1103/PhysRevC.91.014303

Nuclear breathing mode in neutron-rich Nickel isotopes: sensitivity to the symmetry energy and the role of the continuum

J. Piekarewicz[1, *]

[1] *Department of Physics, Florida State University, Tallahassee, FL 32306*

(Dated: December 15, 2014)

Background: In this new era of radioactive beam facilities, the discovery of novel modes of excitation in nuclei far away from stability represents an area of intense research activity. In addition, some of these modes of excitation, particularly the isoscalar monopole and isovector dipole resonances, appear to be sensitive to the uncertain density dependence of the symmetry energy.

Purpose: It is the main goal of this paper to examine the emergence, evolution, and nature of both the soft and giant isoscalar monopole modes as a function of neutron excess in three unstable Nickel isotopes: ^{56}Ni, ^{68}Ni, and ^{78}Ni.

Methods: The distribution of isoscalar monopole strength is computed in a relativistic random-phase approximation using several accurately calibrated effective interactions. In particular, a non-spectral Green's function approach is adopted that allows for an exact treatment of the continuum without any reliance on discretization. The discretization of the continuum is neither required nor admitted.

Results: In the case of ^{56}Ni, the lack of low-energy strength results in a direct correlation between the centroid energy of the giant monopole resonance and the incompressibility coefficient of symmetric nuclear matter. In contrast, the large neutron excess in both ^{68}Ni and ^{78}Ni generates a significant, yet relatively featureless, amount of low-energy strength that is driven by transitions into the continuum. Moreover, the evolution of monopole strength with neutron excess displays sensitivity to the density dependence of the symmetry energy.

Conclusions: It is suggested that future measurements of the distribution of isoscalar monopole strength at radioactive beam facilities using a very long chain of both stable and unstable isotopes could place important constraints on the equation of state of neutron-rich matter and ultimately on the properties of neutron stars. However, given the nature of the low-energy monopole excitations, a proper treatment of the continuum is absolutely essential.

PACS numbers: 21.60.Jz, 24.10.Jv, 24.30.Cz

* jpiekarewicz@fsu.edu

I. INTRODUCTION

Fundamental new discoveries at radioactive beam facilities all over the world have led to a paradigm shift in nuclear structure. Core concepts that have endured the test of time, such as the traditional magic numbers, are being revisited and revised. This newly discovered fragility of magic numbers only becomes apparent far away from the line of stability. Thus, exotic neutron-rich nuclei have opened a new window into the elusive isovector sector of the nuclear energy density functional (EDF). Moreover, some of these discoveries are providing meaningful constraints on the behavior of neutron-rich matter, whose equation of state (EOS) is essential for the understanding of complex astrophysical objects such as core-collapse supernovae and neutron stars. Such advances in terrestrial laboratories together with the advent of powerful land- and spaced-based telescopes operating at a variety of wavelengths have created a unique and special synergy between nuclear physics and astrophysics.

A ground-state observable that is highly sensitive to the EOS of neutron-rich matter—particularly to the density dependence of the symmetry energy—is the the neutron-skin thickness of ^{208}Pb. Indeed, despite the enormous difference in scales, an accurate measurement of the neutron skin of ^{208}Pb may provide vital insights into the structure of neutron stars [1–11]. The Lead Radius Experiment ("PREX") at the Jefferson Laboratory has provided the first model-independent evidence in favor of a neutron-rich skin in ^{208}Pb [12, 13]. This pioneering experiment—that will soon be upgraded to achieve the originally proposed precision—measures a parity-violating asymmetry in elastic electron scattering. Such a purely electroweak measurement is a sensitive probe of neutron densities that is free from large and uncontrolled strong-interaction uncertainties. Moreover, PREX may serve as an anchor to calibrate future hadronic measurements of neutron skins of exotic nuclei at rare isotope facilities.

Whereas the ground-state properties of exotic nuclei are of great value in constraining the nuclear EDF, elucidating the full complexity of the nuclear dynamics requires a comprehensive study of the response of the nuclear ground state to a variety of probes. Indeed, nuclear resonances offer a unique view of the nucleus that is often inaccessible through any other means [14]. In this new era of radioactive beam facilities the study of novel modes of excitation in exotic nuclei is a rapidly evolving area that holds great promise for new discoveries [15]. Although interesting in their own right, giant and pygmy resonances are also enormously valuable in providing stringent constraints on the equation of state of asymmetric matter [16]. In particular, the electric dipole polarizability $\alpha_{\rm D}$ has been shown to be highly sensitive to the density dependence of the symmetry energy [17–20]. This realization, in combination with a landmark measurement of $\alpha_{\rm D}$ in ^{208}Pb at the Research Center for Nuclear Physics [21, 22], suggests that a comprehensive program of experimental measurements of $\alpha_{\rm D}$ on a variety of nuclei will place important constraints on the isovector sector of the nuclear EDF.

Although primarily sensitive to the incompressibility coefficient of symmetric nuclear matter, the isoscalar giant monopole resonance—particularly in heavy nuclei with a significant neutron excess—is also sensitive to the density dependence of the symmetry energy because it probes the incompressibility of neutron-rich matter [23]. Unfortunately, this sensitivity is hindered by the relatively small neutron excess of the stable nuclei measured up to date. Hence, measuring the isotopic dependence of the isoscalar giant monopole resonance (ISGMR) for both stable and unstable nuclei is highly desirable. Thus, the recent report of a measurement of the isoscalar monopole response of the unstable neutron-rich ^{68}Ni isotope by Vandebrouck and collaborators represents an important milestone [24].

Pioneering experiments at GSI Helmholtzzentrum für Schwerionenforschung have already measured the distribution of *isovector dipole* strength in ^{68}Ni [25, 26]. These experiments have provided important insights into the emergence of low-energy dipole strength in exotic nuclei and have also been used to constrain critical parameters of the EOS, primarily the slope of the symmetry energy at saturation density [18, 27]. In particular, the identification of the electric dipole polarizabilty as a strong isovector indicator by Reinhard and Nazarewicz [17, 28] has provided an observable whose precise experimental determination could reduce theoretical uncertainties in the EOS. Given that the electric dipole polarizability is proportional to the *inverse* energy weighted sum, the soft dipole mode (the so-called "Pygmy" dipole resonance) plays a predominant role. Indeed, in the particular case of ^{68}Ni, the soft dipole mode appears to exhaust as much as 25% of the total dipole polarizability [18]. Thus, the soft dipole mode has generated considerable excitement as both a novel mode of excitation in exotic nuclei and as a possible constraint on the EOS [27, 29–33]; for a recent comprehensive review on the Pygmy Dipole Resonance see Ref. [34].

However, it is essential to note that the origin of the distribution of low-energy strength in the isoscalar monopole and isovector dipole response is radically different. These differences are now underscored in the context of the random-phase approximation (RPA) framework that is used in most self-consistent calculations of the strength distribution. Any RPA calculation starts by generating a variety of ground-state properties that include single-particle energies, the corresponding single-particle orbitals, and the resulting mean-field potentials. With this information at hand, one constructs the uncorrelated *polarization propagator* that consists of all particle-hole excitations with the spin and parity of the excited state under consideration [35], i.e., 0^+ for the monopole and 1^- for the dipole. In the particular case of the monopole response, this involves $2\hbar\omega$ excitations connecting a particle to a hole with identical quantum numbers (e.g., $2s^{1/2} \rightarrow 3s^{1/2}$). Thus, stable nuclei with strongly-bound orbitals display little (or no) uncorrelated low-energy

monopole strength. This is in contrast with dipole excitations that involve $1\hbar\omega$ excitations and thus particle and hole states that could be relatively close in energy (e.g., $2p^{1/2} \rightarrow 3s^{1/2}$). Once the uncorrelated polarization propagator is obtained, the RPA response emerges from the mixing of all relevant particle-hole excitation via a residual interaction that must be consistent with the one used to generate the ground state. For isoscalar modes, the residual particle-hole interaction is attractive and yields a collective response that consists largely of a single fragment—the giant monopole resonance—that exhausts most of the monopole strength. Although the isovector residual interaction is repulsive, thereby leading to a hardening and quenching of the response, for stable nuclei the final outcome is similar, namely, a giant dipole resonance that exhausts most of the classical energy weighted sum rule. However, as the nucleus becomes neutron-rich, the isovector interaction that played a relatively minor role in the ground-state properties of nuclei with a small neutron excess, generates a significantly repulsive contribution to the neutron mean-field potential. This leads to weakly bound neutron orbitals that in some cases may be close to the continuum. Even so, in the case of the dipole response there may be several discrete excitations in which both the particle and the hole remain bound. In principle, these soft excitations can be coherently mixed by the residual interaction and ultimately generate a fairly well developed soft (pygmy) dipole resonance.

However, the $2\hbar\omega$ character of the monopole excitations necessarily implies that all low-energy excitations must involve transitions into the continuum. Thus, a correct interpretation of the experimental results obtained by Vandebrouck and collaborators [24] requires a proper treatment of the continuum. In particular, the suggestion of a novel soft monopole mode—largely motivated by RPA predictions that use a discretized continuum—may be premature. Indeed, it now appears that the prediction of low-energy monopole peaks that are well separated from the main giant resonance in the neutron-rich Ni-isotopes [36, 37] may be an artifact of the discretization [38]. In a recent analysis based on Skyrme-RPA calculations that do not involve discretizing the continuum, Hamamoto and Sagawa conclude that "it is very unlikely to have some isoscalar monopole peaks with the width of the order of 1 MeV below the excitation energy of 20 MeV in ^{68}Ni" [38]. In this contribution I report relativistic RPA calculations of the distribution of isoscalar monopole strength with an exact treatment of the continuum for ^{56}Ni, ^{68}Ni, and ^{78}Ni. These results are in full agreement with the conclusions by Hamamoto and Sagawa.

The paper has been organized as follows. In Sec. II a brief description of the relativistic RPA formalism used in this work is presented, paying special attention to the treatment of the continuum. One then proceeds in Sec. III to display predictions for the distribution of isoscalar monopole strength in the isospin symmetric ^{56}Ni nucleus as well as in the neutron-rich isotopes ^{68}Ni and ^{78}Ni. Again, special attention is paid to the role of the continuum in dictating the shape of the low-energy strength. Finally, Sec. IV contains a summary of the main results.

II. FORMALISM

In this section a brief review is provided of both the formalism required to compute the isoscalar monopole response and the physics that this mode is sensitive to. In the case of the response, special emphasis is placed on the importance of a proper treatment of the continuum. Moreover, although it is well known that the nuclear "breathing" mode probes the incompressibility coefficient of symmetric nuclear matter [14, 39, 40], it is underscored that the monopole response of nuclei with a significant neutron excess is also sensitive to the poorly constrained density dependence of the symmetry energy.

A. Isoscalar Monopole Response

The formalism underlying the calculation of the relativistic mean-field ground state and the corresponding linear response has been reviewed extensively in earlier publications [16, 41, 42]. Although a full review of the formalism is no longer necessary, I nevertheless highlight those points that are of relevance to the present work, specifically the impact of the continuum on the distribution of low-energy isoscalar monopole strength.

In the relativistic mean-field (RMF) approach pioneered by Serot and Walecka [43, 44] the basic constituents of the effective theory are protons and neutrons interacting via the exchange of various mesons and the photon. In addition to these conventional Yukawa terms, the model is supplemented by a variety of nonlinear meson coupling terms that are critical to improve the quality of the model [1, 45, 46]. In the RMF approximation, the nucleons satisfy a Dirac equation in the presence of strong scalar and vector potentials that are generated by the meson fields. In turn, the mesons and the photon satisfy classical Klein-Gordon equations with the relevant nuclear densities acting as source term. Due to this close interdependence, the equations of motion must be solved self-consistently until convergence is attained [47]. The self-consistent procedure culminates with the determination of single-particle energies and Dirac wave-functions, ground-state densities, and meson fields.

With such information at hand, one may proceed to compute the linear response of the mean-field ground state to a weak external perturbation. In the language of many-body theory, this requires the evaluation of the *polarization propagator* [35, 48]. The polarization propagator—which is a function of both the energy and momentum transfer to the nucleus—contains all dynamical information relevant to the excitation spectrum of the system. Indeed, the polarization propagator is an analytic function of the energy transfer except for simple poles located at the excitation energies of the system and with the residues at the pole corresponding to the transition form factor. The first step in the calculation of the isoscalar monopole response is the construction of the *uncorrelated* (or mean-field) polarization propagator that is given by the following expression:

$$\begin{aligned}\Pi_{ab}(\mathbf{x},\mathbf{y};\omega) = & \sum_{0<n<F} \overline{U}_n(\mathbf{x})\gamma^0\tau_a G_F\Big(\mathbf{x},\mathbf{y};+\omega+E_n^{(+)}\Big)\gamma^0\tau_b\, U_n(\mathbf{y}) \\ & + \sum_{0<n<F} \overline{U}_n(\mathbf{y})\gamma^0\tau_b G_F\Big(\mathbf{y},\mathbf{x};-\omega+E_n^{(+)}\Big)\gamma^0\tau_a\, U_n(\mathbf{x})\,, \end{aligned} \tag{1}$$

where $E_n^{(+)}$ and $U_n(\mathbf{x})$ are the single-particle energies and Dirac wave-functions obtained from the self-consistent determination of the mean-field ground state, $\gamma^0 = \mathrm{diag}(1,1,-1,-1)$ is the zeroth component of the Dirac matrices, τ_0 is the identity matrix in isospin space, and $\tau_3 = \mathrm{diag}(1,-1)$ is the third isospin matrix. Note that the sum is restricted to positive-energy states below the Fermi level. Central to the calculation of the polarization propagator Π_{ab} is the single-nucleon propagator $G(\mathbf{x},\mathbf{y};\omega)$. The nucleon mean-field propagator differs from its free-space value in two important ways. First, the propagating nucleon interacts with the average mean-field potential generated by the nuclear medium. Second, at finite density the presence of a filled Fermi sea modifies the analytic structure of the free propagator [44] (see also Fig.1 in Ref. [16]). This suggests the following decomposition of the nucleon propagator:

$$G(\mathbf{x},\mathbf{y};\omega) = G_F(\mathbf{x},\mathbf{y};\omega) + G_D(\mathbf{x},\mathbf{y};\omega)\,. \tag{2}$$

The "Feynman" part of the propagator G_F admits a spectral decomposition that makes its content particularly simple and illuminating. In terms of the mean-field solutions to the Dirac equation it is given by

$$G_F(\mathbf{x},\mathbf{y};\omega) = \sum_n \left(\frac{U_n(\mathbf{x})\overline{U}_n(\mathbf{y})}{\omega - E_n^{(+)} + i\eta} + \frac{V_n(\mathbf{x})\overline{V}_n(\mathbf{y})}{\omega + E_n^{(-)} - i\eta} \right)\,, \tag{3}$$

where now $E_n^{(-)}$ and $V_n(\mathbf{x})$ represent single-particle energies and Dirac wave-functions associated with the negative-energy part of the spectrum; recall that in the relativistic formalism the positive energy part of the spectrum by itself is not complete. Note that the sum is now unrestricted, as it involves bound and continuum states of both positive and negative energy. In turn, the "density" part of the propagator G_D *corrects* G_F for the presence of a filled Fermi sea. Formally, one effects this correction by shifting the position of the singularity (i.e., simple pole) of every occupied nucleon state from below to above the real axis [16, 42]. This yields

$$G_D(\mathbf{x},\mathbf{y};\omega) = 2\pi i \sum_{n<\mathrm{F}} \delta\Big(\omega - E_n^{(+)}\Big) U_n(\mathbf{x})\overline{U}_n(\mathbf{y}). \tag{4}$$

In this manner, the uncorrelated polarization propagator displayed in Eq.(1), and depicted graphically by the thin blue "bubble" in Fig.1, involves a product of two such nucleon propagators that accounts for all particle-hole excitations. However, it is important to underline that consistency with the mean-field approximation adopted here demands that *vacuum polarization*, namely, the divergent bubble diagram resulting from the product of two Feynman propagators G_F, be neglected.

Although the spectral decomposition of the single-nucleon propagator is highly illuminating, its use in the calculation of the polarization propagator introduces certain artificial features—such as an energy cutoff and the discretization of the continuum—that may produce unreliable results. To avoid any reliance on artificial cutoffs and truncations, it is convenient to compute the nucleon propagator *non-spectrally* by solving exactly for the relevant Green's function. That is,

$$\Big(\omega\gamma^0 + i\boldsymbol{\gamma}\cdot\boldsymbol{\nabla} - M - \Sigma_{\mathrm{MF}}(\mathbf{x})\Big) G_F(\mathbf{x},\mathbf{y};\omega) = \delta(\mathbf{x}-\mathbf{y})\,, \tag{5}$$

where $\boldsymbol{\gamma} = (\gamma^1,\gamma^2,\gamma^3)$ are Dirac gamma matrices and Σ_{MF} is the *same exact* mean-field potential obtained from the self-consistent solution of the ground-state problem. Note that it is only by ensuring that both the bound single-particle wave functions U_n and the nucleon propagator G_F "move" under the influence of the same mean-field potential

that the conservation of the vector current can be ensured [42]. Moreover, the nonspectral approach has the enormous advantage that both the positive- and negative-energy continua are treated exactly.

Having generated the mean-field polarization propagator, one proceeds to build coherence into the nuclear response by mixing all particle-hole excitations of the same spin and parity. Such a procedure is implemented by iterating the uncorrelated polarization propagator to all orders. The resulting RPA response often displays strong collective behavior that manifests itself in the appearance of one "giant resonance" that exhausts most of the classical sum rule [14]. Besides its enormous impact on building the observed collectivity of certain nuclear modes, RPA correlations embody the correct self-consistent response of the mean-field ground state [49–51]. In particular, in a seminal paper on vibrational states in nuclei, Thouless showed how spurious states—such as those associated with a uniform translation of the center-of-mass—separate out cleanly from the physical modes by shifting the spurious strength to zero excitation energy [49]. In the context of the relativistic formalism, Dawson and Furnstahl generalized Thouless' result by placing particular emphasis on the role of the negative-energy states in the quest for consistency [50].

By introducing the Fourier transform of the mean-field polarization propagator,

$$\Pi_{ab}(\mathbf{q},\mathbf{q}';\omega)=\int d^3x\, d^3y\, e^{-i(\mathbf{q}\cdot\mathbf{x}-\mathbf{q}'\cdot\mathbf{y})}\,\Pi_{ab}(\mathbf{x},\mathbf{y};\omega)\,, \tag{6}$$

one can obtain Dyson's equation for the RPA polarization whose solution encapsulates the collective response of the mean-field ground state. That is,

$$\Pi^{\rm RPA}_{ab}(\mathbf{q},\mathbf{q}';\omega)=\Pi_{ab}(\mathbf{q},\mathbf{q}';\omega)+\int\frac{d^3k}{(2\pi)^3}\frac{d^3k'}{(2\pi)^3}\Pi_{ac}(\mathbf{q},\mathbf{k};\omega)V_{cd}(\mathbf{k},\mathbf{k}';\omega)\Pi^{\rm RPA}_{db}(\mathbf{k}',\mathbf{q}';\omega)\,, \tag{7}$$

where $V_{cd}(\mathbf{k},\mathbf{k}';\omega)$ is the residual particle-hole interaction. The diagrammatic representation of the RPA equations is displayed in Fig. 1. It is worth repeating that the consistent linear response of the system requires that both the mean-field potential $\Sigma_{\rm MF}$ and the residual particle hole interaction V_{ab} be consistent with the interaction used to generate the mean-field ground state.

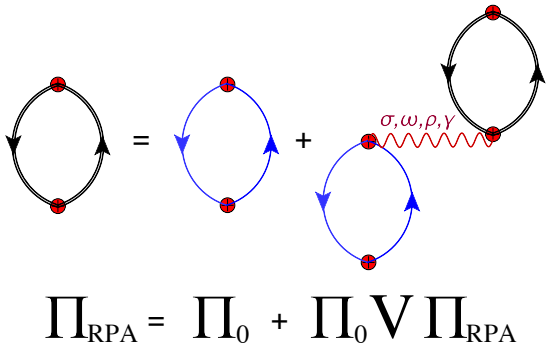

FIG. 1. (Color online) Diagrammatic representation of the RPA (or Dyson's) equations. The ring diagram with the thick black lines represents the fully correlated RPA polarization while the one depicted with the thin blue lines is the uncorrelated mean-field polarization. The residual interaction denoted with the red wavy line must be identical to the one used to generate the mean-field ground state.

Finally, the distribution of isoscalar monopole strength may be obtained by taking the imaginary part of the polarization propagator projected into the correct $(J^\pi=0^+,T=0)$ channel. That is,

$$S(q,\omega;E0)=-\frac{1}{\pi}{\rm Im}\Big(\Pi^{\rm RPA}_{00}(\mathbf{q},\mathbf{q};\omega)\Big)\,. \tag{8}$$

In the long wavelength limit, the distribution of isoscalar monopole strength $R(\omega;E0)$ reduces to the following expression:

$$R(\omega;E0)=\lim_{q\to0}\left(\frac{36}{q^4}\right)S(q,\omega;E0)\,. \tag{9}$$

In turn, moments of the distribution are defined as suitable energy weighted sums, namely,

$$m_n(E0)\equiv\int_0^\infty\omega^n R(\omega;E0)\,d\omega\,. \tag{10}$$

Widely used in the literature are the energy weighted m_1, the energy unweighted m_0, and the inverse energy weighted m_{-1} sums [14].

B. Incompressibility of Neutron-Rich Matter

The saturation of infinite nuclear matter, namely, the existence of an equilibrium density, is a hallmark of the complex and rich nuclear dynamics. Given that the pressure vanishes at the equilibrium density, the small density fluctuations around saturation are described entirely by the incompressibility coefficient of symmetric nuclear matter K_0. Although K_0 can not be measured directly in the laboratory, it can be tightly constrained from the strength distribution of the isoscalar monopole resonance. Indeed, using a sum-rule approach and assuming that all the strength is concentrated in one collective peak, the energy of the isoscalar giant monopole resonance (ISGMR) may be written as follows [14, 52]:

$$E_{\rm GMR} = \sqrt{\frac{\hbar^2 K_A}{M\langle r^2\rangle}}\,, \tag{11}$$

where M is the nucleon mass, $\langle r^2\rangle$ the mean-square nuclear radius, and K_A the *finite-nucleus* incompressibility coefficient. It is important to note that although highly suggestive, modern theoretical approaches do not rely on the above expression to infer the value of K_0. Rather, the same energy density functional is used to predict both K_0 and the distribution of isoscalar monopole strength.

Besides providing vital information on the equation of state of symmetric nuclear matter, the ISGMR of nuclei with a large neutron excess could shed light on the density dependence of the symmetry energy. Indeed, to the extent that the ISGMR probes the incompressibility of infinite nuclear matter, the monopole response of nuclei with a significant neutron excess should be sensitive to the incompressibility coefficient of *neutron-rich matter* [23]. To quantify the sensitivity of the symmetry energy to the ISGMR, it is convenient to introduce the energy per particle of asymmetric nuclear matter at zero temperature as follows:

$$E/A(\rho,\alpha) - M \equiv \mathcal{E}(\rho,\alpha) = \mathcal{E}_{\rm SNM}(\rho) + \alpha^2\mathcal{S}(\rho) + \mathcal{O}(\alpha^4)\,, \tag{12}$$

where $\rho = \rho_n + \rho_p$ is the total (neutron plus proton) baryon density, $\mathcal{E}_{\rm SNM}$ is the energy per particle of symmetric nuclear matter, $\mathcal{S}$ is the symmetry energy, and $\alpha = (\rho_n - \rho_p)/\rho$ represents the neutron-proton asymmetry. If one now expands the energy per particle around saturation density ($\rho_{\rm o}$) one obtains

$$\mathcal{E}(\rho,\alpha) = \Big(\varepsilon_{\rm o} + \frac{1}{2}K_0x^2 + \frac{1}{6}Q_0x^3 + \ldots\Big) + \alpha^2\Big(J + Lx + \frac{1}{2}K_{\rm sym}x^2 + \frac{1}{6}Q_{\rm sym}x^3 + \ldots\Big)\,, \tag{13}$$

where $x = (\rho - \rho_{\rm o})/3\rho_{\rm o}$ describes the deviation of the density from its value at saturation. Here $\varepsilon_{\rm o}$, K_0, and Q_0 denote the binding energy per nucleon, curvature (i.e., incompressibility), and skewness parameter of symmetric nuclear matter; J, $K_{\rm sym}$, and $Q_{\rm sym}$ represent the corresponding quantities for the symmetry energy. Note, however, that unlike symmetric nuclear matter, the symmetry pressure—or equivalently the slope of the symmetry energy L—does not vanish. This suggests that whereas symmetric nuclear matter ($\alpha \equiv 0$) saturates at $\rho_{\rm o}$, the presence of L modifies the saturation properties of asymmetric matter. Indeed, the following analytic expressions (correct to second order in α) summarize the saturation properties of *asymmetric nuclear matter* [23]:

$$\rho_{\rm o}(\alpha) = \rho_{\rm o} + \rho_\tau\alpha^2 = \rho_{\rm o}\left(1 - 3\frac{L}{K_0}\alpha^2\right)\,, \tag{14a}$$

$$\varepsilon_{\rm o}(\alpha) = \varepsilon_{\rm o} + \varepsilon_\tau\alpha^2 = \varepsilon_{\rm o} + J\alpha^2\,, \tag{14b}$$

$$K_0(\alpha) = K_0 + K_\tau\alpha^2 = K_0 + \Big(K_{\rm sym} - 6L - \frac{Q_0}{K_0}L\Big)\alpha^2\,. \tag{14c}$$

Note that on very general grounds—both theoretical from the dynamics of pure neutron matter [53–59] and a variety of correlation studies [60–63], as well as experimental from a measurement of the neutron-rich skin in ^{208}Pb [12, 13], the value of the slope of the symmetry energy L has been constrained to be positive. As a result, Eq. (14a) indicates that neutron-rich matter saturates at lower densities. Moreover, although slightly more uncertain, the correction term to the incompressibility coefficient (K_τ) appears also to be negative, as it is dominated by the slope of the symmetry energy [16, 23]; see the large factor of 6 in front of L in Eq. (14c). This suggests that measurements of the isotopic dependence of the giant monopole resonance—that should include unstable nuclei with a very large neutron excess—could place significant constraints on the density dependence of the symmetry energy. Important first steps in this direction have been already taken by Garg and collaborators [64–66]. In the present paper the focus is shifted to the unstable neutron-rich isotopes ^{68}Ni and ^{78}Ni, with neutron-proton asymmetries of $\alpha_{68} = 0.18$ and $\alpha_{78} = 0.28$, respectively.

III. RESULTS

Having provided the necessary framework to compute the distribution of isoscalar monopole strength and having discussed the physics that this mode is sensitive to, predictions are now displayed for three relativistic mean-field models: (a) NL3 [67, 68], FSUGold [69], and IUFSU [70]. Whereas both NL3 and FSUGold are accurately-calibrated interactions, IUFSU involves a fine tuning of FSUGold in response to an interpretation of x-ray observations of neutron stars that suggest that FSUGold predicts stellar radii that are too large and a maximum stellar mass that is too small [71]. Model parameters (i.e., coupling constants and meson masses) for these three sets of interactions have been listed in Table I of Ref. [70].

Earlier attempts aimed at connecting the energies of the GMR to the incompressibility coefficient K_0 relied heavily on dangerous extrapolations from the properties of finite nuclei to those of infinite nuclear matter [39, 40]. However, as a result of the much stricter standards imposed on the field today, predictions for a variety of bulk properties of infinite nuclear matter as well as the distribution of isoscalar monopole strength may now be provided without any recourse to semi-empirical mass formulas. In Table I predictions are listed for a variety of bulk properties of infinite nuclear matter at saturation density ρ_0 as defined in Eq. (13). In particular, ε_0, K_0, and Q_0 represent the binding energy per nucleon, the incompressibility coefficient, and skewness parameter of symmetric nuclear matter, while J, L, and $K_{\rm sym}$ represent the energy, slope, and curvature of the symmetry energy. From these quantities, one can then obtain the asymmetric contribution to the incompressibility coefficient K_τ, as per Eq. (14c). Finally, K_{56}, K_{68}, and K_{78} represent the incompressibility coefficient of neutron-rich matter having the same neutron excess as ^{56}Ni($\alpha=0$), ^{68}Ni($\alpha=0.18$), and ^{78}Ni($\alpha=0.28$), respectively. Note that although the NL3 prediction for K_0 is significantly larger than for the other two models, the differences disappear almost entirely in the case of K_{78}; i.e., by the time the neutron-proton asymmetry has grown up to $\alpha=0.28$. This is due to the very stiff symmetry energy of NL3 which, in turn, provides a large correction to K_0, i.e., $K_\tau\approx-6L\approx-700$ MeV. Thus, the isotopic dependence of the ISGMR can help elucidate the density dependence of the symmetry energy—provided the isotopic chain includes exotic nuclei with very large neutron-proton asymmetries.

Model	ρ_0	ε_0	K_0	Q_0	J	L	$K_{\rm sym}$	K_τ	K_{56}	K_{68}	K_{78}
NL3	0.148	−16.24	271.5	209.5	37.29	118.2	100.9	−699.4	271.5	249.8	215.9
FSU	0.148	−16.30	230.0	−522.7	32.59	60.5	−51.3	−276.9	230.0	221.4	208.0
IUFSU	0.155	−16.40	231.3	−291.1	31.30	47.2	28.5	−195.3	231.3	225.3	215.8

TABLE I. Bulk parameters characterizing the behavior of infinite nuclear matter at saturation density as defined in Eqs. (13) and (14c). Note that K_{56}, K_{68}, and K_{78} represent the incompressibility coefficient of asymmetric matter with the same neutron excess as ^{56}Ni, ^{68}Ni, and ^{78}Ni, respectively. All quantities are given in MeV except for ρ_0 which is given in fm^{-3}.

Given that the self-consistent calculation of ground-state properties is the necessary first step in the development of the RPA response, listed in Table II are the predictions of all three models for the binding energy per nucleon, root-mean-square charge and neutron radii, and neutron-skin thickness of ^{56}Ni, ^{68}Ni, and ^{78}Ni. As far as one can tell, experimental values exist only for the binding energies [72]. Relative to experiment (experimental results not shown) the largest deviation in the binding energy is obtained in the case of IUFSU: 1.7% for ^{56}Ni, 0.3% for ^{68}Ni, and 1.5% for ^{78}Ni. For the charge radii, where experimental measurements are not yet available, the spread among the predictions amounts to less than half a percent for all three isotopes. However, as a result of the large uncertainty in the value of the slope of the symmetry energy L, a marked discrepancy is observed in the predictions for the neutron radius and neutron-skin thickness of both neutron-rich nuclei. In the case of ^{78}Ni, the difference between the stiffest (NL3) and softest (IUFSU) models is about 0.13 fm. In particular, note that NL3 predicts a very thick neutron skin of $R^{78}_{\rm skin}=0.416$ fm.

	^{56}Ni				^{68}Ni				^{78}Ni			
Model	B/A	$R_{\rm ch}$	R_n	$R_{\rm skin}$	B/A	$R_{\rm ch}$	R_n	$R_{\rm skin}$	B/A	$R_{\rm ch}$	R_n	$R_{\rm skin}$
NL3	8.608	3.701	3.578	−0.049	8.688	3.855	4.045	0.261	8.239	3.934	4.281	0.416
FSU	8.526	3.707	3.581	−0.053	8.664	3.852	3.992	0.210	8.152	3.948	4.221	0.341
IUFSU	8.501	3.680	3.553	−0.053	8.652	3.842	3.949	0.178	8.108	3.930	4.153	0.292

TABLE II. Theoretical predictions for the binding energy per nucleon, charge radius, neutron radius, and neutron-skin thickness of the three Nickel isotopes for NL3 [67, 68], FSUGold [69], and IUFSU [70]. Binding energies are given in MeV and radii in fm.

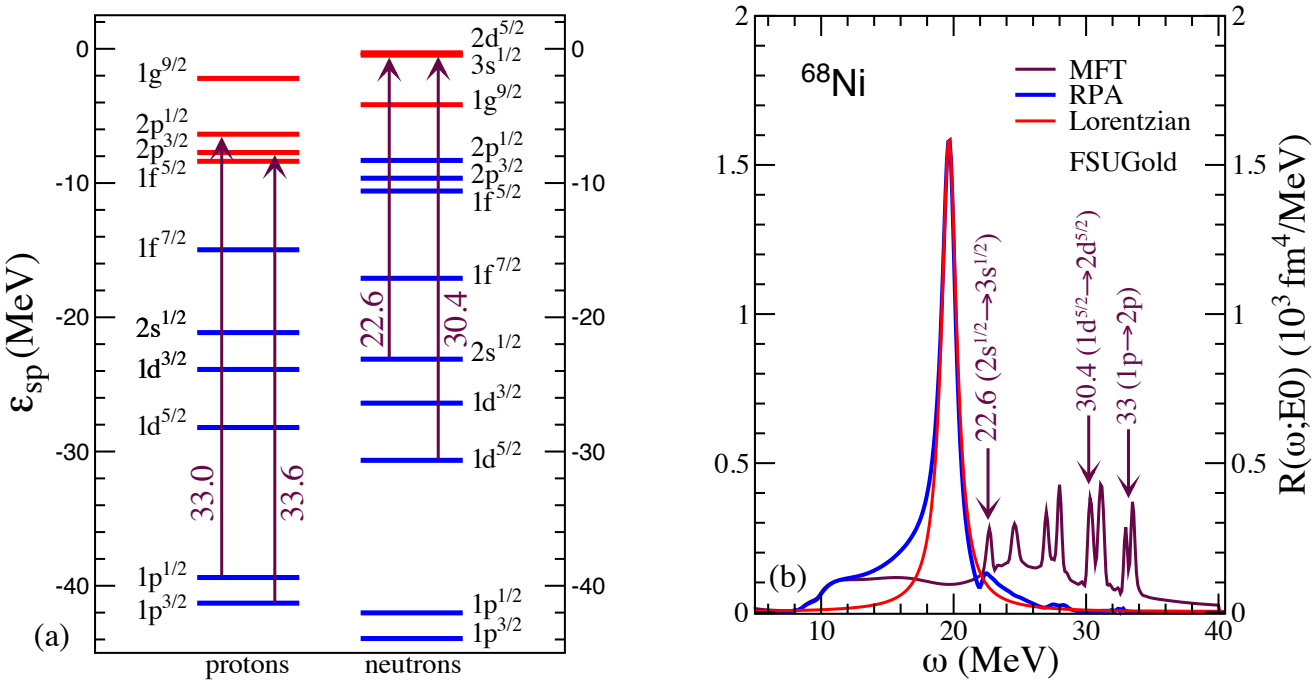

FIG. 2. (Color online) (a) Single-particle spectrum for ^{68}Ni as predicted by the relativistic FSUGold density functional. The blue(red) lines denote occupied(empty) orbitals and the arrows are used to indicate discrete excitations into bound states. (b) Distribution of isoscalar monopole strength for ^{68}Ni as predicted by the relativistic FSUGold density functional. Both uncorrelated (MFT) and correlated (RPA) responses are displayed; the arrows indicate some of the expected mean-field transitions. Also shown is a Lorentzian fit to the giant RPA peak to clearly identify the excess strength at low energy.

Having solved the self-consistent mean-field equations, which yield single-particle energies and Dirac wave-functions as well as the self-consistent scalar and vector mean-fields, one may now compute the distribution of isoscalar monopole strength in a relativistic random-phase approximation [see Eq. (7) and Fig.1]. It is worth repeating that the distribution of monopole strength involves a *non-spectral* solution of the nucleon propagator that is free from any discretization of the continuum. However, in order to resolve discrete particle-hole excitations, namely, excitations in which both the particle and the hole are bound, one must supply the excitation energy ω with a small imaginary part of $\eta \equiv 0.1$ MeV.

In Fig. 2(a) FSUGold predictions are displayed for the single-particle spectrum of ^{68}Ni, with the arrows used to indicate four prominent discrete excitations. As required, these four discrete excitations are also clearly discernible in the distribution of isoscalar monopole strength displayed in Fig. 2(b). Moreover, this uncorrelated (or MFT) response shows a significant amount of fairly structureless strength from about 10 to 20 MeV followed by a series of sharp peaks in the 20 to 35 MeV region. Note that most of the low-energy strength is generated by excitations from a bound Dirac orbital into the continuum. As such, this component of the strength is insensitive to the choice of η (i.e., the small imaginary part of ω). In contrast, the sharp peaks at high-excitation energy represent $2\hbar\omega$ excitations that could not be resolved without such a small imaginary part. Also note the presence of additional "discrete" peaks that are not identified in Fig. 2(a). These extra peaks involve single-particle states at the edge of the continuum, such as the $3s^{1/2}$ and $2d^{5/2}$ proton orbitals.

The attractive isoscalar component of the residual interaction is extremely efficient in mixing all individual particle-hole excitations. This typically results in the development of a single collective peak that exhausts most of the energy weighted sum (EWS) [14]. The appearance of a giant monopole resonance that carries most of the EWS is clearly discernible in Fig. 2(b) (blue solid line). This large collective mode is sensitive to the incompressibility coefficient of infinite nuclear and, at least for stable heavy nuclei, is accurately described by a Lorentzian function. However, in the case of the exotic neutron-rich isotope ^{68}Ni, a significant amount of non-collective excess strength is observed at low energy. This fact is best illustrated by displaying (with a red solid line) a Lorentzian fit to the large collective component. One attributes this difference to the low-energy excitations into the continuum. Note that the shape of the strength distribution at low energies is extremely sensitive to the treatment of the continuum, so one must exercise extreme care in drawing conclusions that rely on its discretization [38].

As just alluded, the nature of the low-energy strength is associated with excitations from valence states into the continuum. As the neutron excess increases, the isovector interaction—which in the relativistic RMF model is dominated by vector exchange—becomes repulsive for the neutrons and attractive for the protons. In the case of ^{68}Ni,

this results in a closely-spaced triplet of orbitals ($1f^{5/2}$, $2p^{3/2}$, and $2p^{1/2}$) with a binding energy of about 10 MeV that hold the 12 extra neutrons relative to ^{56}Ni [see Fig. 2(a)]. This suggests that the emergence of low-energy strength should closely track the neutron excess.

To test this assertion, the distribution of isoscalar monopole strength is displayed in Fig. 3 for ^{56}Ni, ^{68}Ni, and ^{78}Ni as predicted by the RPA calculations. By including three models with different bulk parameters, one can test the sensitivity of the strength distribution to the density dependence of the symmetry energy. Also listed in Table III are various relevant moments of the distribution of strength that were obtained by integrating from $\omega_{\rm min} = 0.5$ MeV to $\omega_{\rm max} = 40$ MeV; see Eq. (10). The lack of low-energy strength in ^{56}Ni is clearly evident in Fig. 3(a). Low-energy

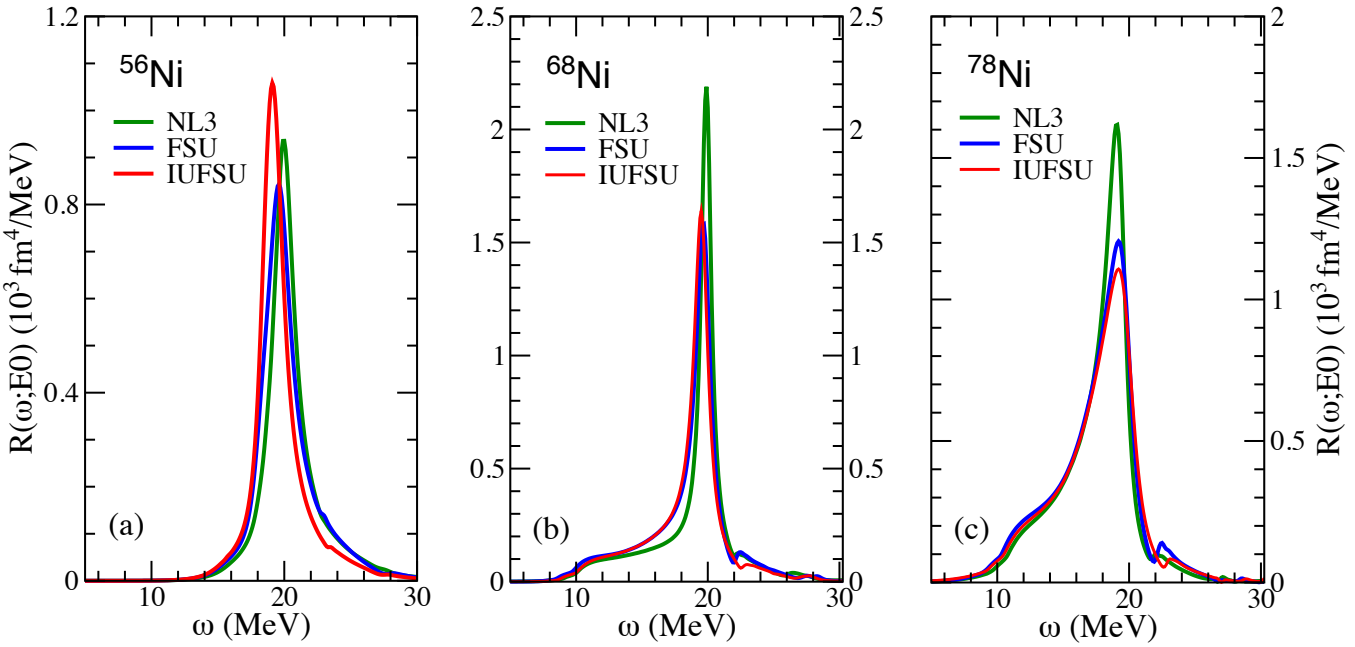

FIG. 3. (Color online) Distribution of isoscalar monopole strength for (a) ^{56}Ni, (b) ^{68}Ni, and (c) ^{78}Ni as predicted by relativistic RPA calculations using NL3 [67, 68], FSUGold [69], and IUFSU [70].

excitations into the continuum that were driven by the neutrons occupying the $1f^{5/2}$, $2p^{3/2}$, and $2p^{1/2}$ orbitals in ^{68}Ni are absent in the case of ^{56}Ni. Further, for a strength distribution dominated by a single collective peak that is well approximated by a Lorentzian shape, resonance energies satisfy the following simple relations:

$$\frac{m_1}{m_0} = \omega_0 \quad \text{and} \quad \sqrt{\frac{m_1}{m_{-1}}} = \omega_0 \sqrt{1 + \frac{\Gamma_0^2}{4\omega_0^2}} \approx \omega_0 \,, \tag{15}$$

where ω_0 and Γ_0 represent the resonance energy and width, respectively. As expected, these relations are well satisfied for the case of ^{56}Ni. However, with the appearance of significant low energy strength in ^{68}Ni—and even more so in ^{78}Ni—significant distortions to the simple Lorentzian shape emerge.

Given that the incompressibility coefficient for symmetric nuclear is largest for NL3, its prediction for the GMR energy of ^{56}Ni is almost one MeV larger than for IUFSU (see Table III). Remarkably, however, the predictions of all three models for the distribution of strength in ^{78}Ni are very similar to each other. This is consistent with the much faster softening of the incompressibility coefficient of neutron-rich matter for NL3 than in the case of either FSUGold or IUFSU; see the value of K_{78} in Table I. Thus, studying the isotopic dependence of the isoscalar monopole resonance for chains containing very exotic nuclei may provide stringent constraints on the density dependence of the symmetry energy [16].

IV. CONCLUSIONS

The unique and fascinating dynamics of exotic neutron-rich nuclei has lead to a paradigm shift in nuclear structure. Besides providing insights into the limits of nuclear existence and the production of heavy elements in the cosmos, the study of nuclei with large isospin asymmetries opens a window into the poorly known nuclear isovector interaction.

Isotope	Model	m_{-1} (fm^4/MeV)	m_0 (fm^4)	m_1 (fm^{4}MeV)	m_3 (fm^{4}MeV^3)	m_1/m_0 (MeV)	$\sqrt{m_1/m_{-1}}$ (MeV)	$\sqrt{m_3/m_1}$ (MeV)
^{56}Ni	NL3	0.138	2.810	58.031	26130.3	20.650	20.498	21.220
	FSU	0.147	2.933	59.487	25850.1	20.283	20.130	20.846
	IUFSU	0.151	2.936	57.996	23763.5	19.752	19.622	20.242
^{68}Ni	NL3	0.239	4.389	83.876	33659.6	19.112	18.751	20.032
	FSU	0.254	4.524	84.045	32020.2	18.577	18.202	19.519
	IUFSU	0.248	4.433	82.080	30795.7	18.516	18.190	19.370
^{78}Ni	NL3	0.358	6.037	105.999	35838.9	17.559	17.199	18.388
	FSU	0.363	6.049	105.532	35687.6	17.446	17.042	18.389
	IUFSU	0.355	5.875	102.612	34849.4	17.466	17.002	18.429

TABLE III. Various moments of the isoscalar monopole strength distribution and corresponding energies for the three Nickel isotopes considered in the text as predicted by NL3 [67, 68], FSUGold [69], and IUFSU [70]. All moments were computed by integrating the distribution of strength from a minimum value of $\omega_{\rm min}=0.5$ MeV to a maximum value of $\omega_{\rm max}=40$ MeV. Note that all the moments—but not their ratios—should be multiplied by a factor of 10^3. For example, the m_0 moment of ^{68}Ni as predicted by FSU should be read as $m_0=4.524\times10^3$ fm^4.

In particular, large nuclei with a significant neutron excess develop a neutron-rich skin that is highly sensitive to the density dependence of the symmetry energy and, consequently, to the nature of the isovector interaction. Moreover, the electric dipole polarizability and the development of low energy pygmy strength in the isovector dipole response display strong sensitivity to the isovector interaction. In the present contribution I have extended the study of the soft dipole mode and its sensitivity to the isovector interaction to the isoscalar monopole response of three magic (or semi-magic) Ni-isotopes—including the two very neutron-rich nuclei ^{68}Ni and ^{78}Ni.

The isotopic dependence of the isoscalar monopole resonance is of great interest because the softening of the mode with increasing neutron excess is highly sensitive to the density dependence of the symmetry energy; see the expression for K_τ in Eq. (14c). Although pioneering measurements of the isotopic dependence of the ISGMR in both Tin and Cadmium have already been carried out, these measurements have been limited to the stable isotopes where the neutron excess, while significant, is not yet sufficiently large. Yet, one is confident that in the new era of rare isotope facilities these experimental studies will be extended much further.

Central to this work was also the study of the emergence of low-energy isoscalar monopole strength as a function of neutron excess. In the case of the isovector dipole resonance, the appearance of low-energy pygmy strength was seen to be strongly correlated to the development of a neutron-rich skin in the Sn-isotopes. And although the nature of the pygmy dipole resonance is still under debate, primarily whether it is collective or not, the emergence of low-energy strength as a result of a significant neutron excess is undeniable.

However, the nature of the isoscalar monopole strength at low energies appears to be significantly more complex. To shed light on this problem, relativistic RPA calculations were carried out for the distribution of isoscalar monopole strength in ^{56}Ni, ^{68}Ni, and ^{78}Ni. In addition, one has used three RMF models with different assumptions on the isovector interaction to test the reliability of the conclusions. Finally and most importantly, the RPA formalism employed here is based on a non-spectral Green's function approach where the continuum is treated on the same footing as the bound states. This is in contrast to spectral calculations that must rely on a discretization of the continuum.

To conclude, a summary of the most important results is now presented. No low energy monopole strength is found in the symmetric ^{56}Ni isotope. Rather, only one single collective giant resonance is identified with a centroid energy located at $m_1/m_0=20.65$ MeV for NL3 (a model with an incompressibility coefficient of $K_0\approx270$ MeV) and at 19.75 MeV for IUFSU (with $K_0\approx230$ MeV). However, in contrast to the case of ^{56}Ni, a significant amount of low-energy strength is observed in both neutron-rich isotopes ^{68}Ni and ^{78}Ni—especially in the case of the latter. Such structureless strength is associated with the excitation of the extra 12 and 22 neutrons into the continuum. In the absence of RPA correlations, the shape of the mean-field response consists of featureless strength from about 10 to 20 MeV followed by discrete particle-hole excitations in the 20 to 35 MeV region. Once the attractive residual interaction is incorporated, the coherence among all particle-hole excitations gives rise to an RPA response that is significantly softened and enhanced. This yields a smooth distribution of isoscalar monopole strength that in addition to the giant resonance peak displays a significant amount of low-energy strength. However, unlike some of the results obtained using a discretized continuum, no pronounced monopole states in the low-energy region that are well separated from the giant monopole resonance are found [37]. Instead, the results found here support the recent *continuum* calculations by Hamamoto and Sagawa that report a "broad shoulder" of low-energy monopole strength and question the appearance of isoscalar monopole peaks below 20 MeV [38]. Given that a proper treatment of the continuum is absolutely critical, the possible indication of a soft monopole mode in ^{68}Ni located at an energy of

12.9 ± 1.9 MeV [24], and largely motivated by the predictions of Ref. [37], may need further verification and validation.

ACKNOWLEDGMENTS

The author wishes to express his enormous gratitude to Professor Elias Khan for his support and hospitality during a recent visit to IPN-Orsay where some of the ideas presented in this contribution were first discussed. This material is based upon work supported by the U.S. Department of Energy Office of Science, Office of Nuclear Physics under Award Number DE-FD05-92ER40750.

[1] C. J. Horowitz and J. Piekarewicz, Phys. Rev. Lett. **86**, 5647 (2001).
[2] C. J. Horowitz and J. Piekarewicz, Phys. Rev. **C64**, 062802 (2001).
[3] C. J. Horowitz and J. Piekarewicz, Phys. Rev. **C66**, 055803 (2002).
[4] J. Carriere, C. J. Horowitz, and J. Piekarewicz, Astrophys. J. **593**, 463 (2003).
[5] A. W. Steiner, M. Prakash, J. M. Lattimer, and P. J. Ellis, Phys. Rept. **411**, 325 (2005).
[6] B.-A. Li and A. W. Steiner, Phys. Lett. **B642**, 436 (2006).
[7] J. M. Lattimer and M. Prakash, Phys. Rept. **442**, 109 (2007).
[8] J. M. Lattimer, Ann. Rev. Nucl. Part. Sci. **62**, 485 (2012).
[9] J. Erler, C. J. Horowitz, W. Nazarewicz, M. Rafalski, and P.-G. Reinhard, Phys.Rev. **C87**, 044320 (2013).
[10] F. J. Fattoyev and J. Piekarewicz, Phys. Rev. **C88**, 015802 (2012).
[11] C. J. Horowitz, E. Brown, Y. Kim, W. Lynch, R. Michaels, *et al.*, J. Phys. **G41**, 093001 (2014).
[12] S. Abrahamyan, Z. Ahmed, H. Albataineh, K. Aniol, D. Armstrong, *et al.*, Phys. Rev. Lett. **108**, 112502 (2012).
[13] C. J. Horowitz, Z. Ahmed, C. Jen, A. Rakhman, P. Souder, *et al.*, Phys. Rev. **C85**, 032501 (2012).
[14] M. N. Harakeh and A. van der Woude, "Giant resonances-fundamental high-frequency modes of nuclear excitation," (Clarendon, Oxford, 2001).
[15] N. Paar, D. Vretenar, E. Khan, and G. Colò, Rept. Prog. Phys. **70**, 691 (2007).
[16] J. Piekarewicz, Eur. Phys. J. A **50**, 25 (2013).
[17] P.-G. Reinhard and W. Nazarewicz, Phys. Rev. **C81**, 051303 (2010).
[18] J. Piekarewicz, Phys. Rev. **C83**, 034319 (2011).
[19] J. Piekarewicz, B. Agrawal, G. Colò, W. Nazarewicz, N. Paar, *et al.*, Phys. Rev. **C85**, 041302(R) (2012).
[20] X. Roca-Maza, M. Centelles, X. Vias, M. Brenna, G. Colò, *et al.*, Phys. Rev. **C88**, 024316 (2013).
[21] A. Tamii *et al.*, Phys. Rev. Lett. **107**, 062502 (2011).
[22] I. Poltoratska, P. von Neumann-Cosel, A. Tamii, T. Adachi, C. Bertulani, et al., Phys. Rev. **C85**, 041304 (2012).
[23] J. Piekarewicz and M. Centelles, Phys. Rev. **C79**, 054311 (2009).
[24] M. Vandebrouck, J. Gibelin, E. Khan, N. Achouri, H. Baba, *et al.*, Phys. Rev. Lett. **113**, 032504 (2014).
[25] O. Wieland *et al.*, Phys. Rev. Lett. **102**, 092502 (2009).
[26] D. Rossi, P. Adrich, F. Aksouh, H. Alvarez-Pol, T. Aumann, *et al.*, Phys. Rev. Lett. **111**, 242503 (2013).
[27] A. Carbone, G. Colò, A. Bracco, L.-G. Cao, P. F. Bortignon, *et al.*, Phys. Rev. **C81**, 041301 (2010).
[28] P.-G. Reinhard and W. Nazarewicz, Phys. Rev. **C87**, 014324 (2013).
[29] N. Tsoneva, H. Lenske, and C. Stoyanov, Phys. Lett. **B586**, 213 (2004).
[30] J. Piekarewicz, Phys. Rev. **C73**, 044325 (2006).
[31] N. Tsoneva and H. Lenske, Phys. Rev. **C77**, 024321 (2008).
[32] A. Klimkiewicz *et al.*, Phys. Rev. **C76**, 051603 (2007).
[33] P. Papakonstantinou, H. Hergert, V. Y. Ponomarev, and R. Roth, Phys. Rev. **C89**, 034306 (2014).
[34] D. Savran, T. Aumann, and A. Zilges, Prog. Part. Nucl. Phys. **70**, 210 (2013).
[35] W. H. Dickhoff and D. Van Neck, "Many-body theory exposed," (World Scientific Publishing Co., 2005).
[36] L. Capelli, G. Colò, and J. Li, Phys. Rev. **C79**, 054329 (2009).
[37] E. Khan, N. Paar, and D. Vretenar, Phys. Rev. **C84**, 051301 (2011).
[38] I. Hamamoto and H. Sagawa, (2014), arXiv:1408.6007 [nucl-th].
[39] J. P. Blaizot, Phys. Rept. **64**, 171 (1980).
[40] J. Blaizot, J. Berger, J. Decharge, and M. Girod, Nucl. Phys. **A591**, 435 (1995).
[41] J. Piekarewicz, Phys. Rev. **C62**, 051304 (2000).
[42] J. Piekarewicz, Phys. Rev. **C64**, 024307 (2001).
[43] J. D. Walecka, Annals Phys. **83**, 491 (1974).
[44] B. D. Serot and J. D. Walecka, Adv. Nucl. Phys. **16**, 1 (1986).
[45] J. Boguta and A. R. Bodmer, Nucl. Phys. **A292**, 413 (1977).
[46] H. Mueller and B. D. Serot, Nucl. Phys. **A606**, 508 (1996).
[47] B. G. Todd and J. Piekarewicz, Phys. Rev. **C67**, 044317 (2003).
[48] A. L. Fetter and J. D. Walecka, "Quantum theory of many particle systems," (McGraw-Hill, New York, 1971).

[49] D. Thouless, Nuclear Physics **22**, 78 (1961).
[50] J. F. Dawson and R. J. Furnstahl, Phys. Rev. **C42**, 2009 (1990).
[51] P. Ring and P. Schuck, "The nuclear many-body problem," (Springer, New York, 2004).
[52] S. Stringari, Phys. Lett. **B108**, 232 (1982).
[53] A. Schwenk and C. J. Pethick, Phys. Rev. Lett. **95**, 160401 (2005).
[54] K. Hebeler and A. Schwenk, Phys. Rev. **C82**, 014314 (2010).
[55] A. Gezerlis and J. Carlson, Phys. Rev. **C81**, 025803 (2010).
[56] I. Vidana, C. Providencia, A. Polls, and A. Rios, Phys. Rev. **C80**, 045806 (2009).
[57] S. Gandolfi, A. Y. Illarionov, K. Schmidt, F. Pederiva, and S. Fantoni, Phys. Rev. **C79**, 054005 (2009).
[58] I. Tews, T. Krueger, K. Hebeler, and A. Schwenk, Phys. Rev. Lett. **110**, 032504 (2013).
[59] S. Gandolfi, J. Carlson, S. Reddy, A. Steiner, and R. Wiringa, Eur. Phys. J. **A50**, 10 (2014).
[60] B. A. Brown, Phys. Rev. Lett. **85**, 5296 (2000).
[61] R. J. Furnstahl, Nucl. Phys. **A706**, 85 (2002).
[62] M. Centelles, X. Roca-Maza, X. Viñas, and M. Warda, Phys. Rev. Lett. **102**, 122502 (2009).
[63] X. Roca-Maza, M. Centelles, X. Vinas, and M. Warda, Phys. Rev. Lett. **106**, 252501 (2011).
[64] T. Li *et al.*, Phys. Rev. Lett. **99**, 162503 (2007).
[65] T. Li *et al.*, Phys. Rev. **C81**, 034309 (2010).
[66] D. Patel, U. Garg, M. Fujiwara, H. Akimune, G. Berg, *et al.*, Phys. Lett. **B718**, 447 (2012).
[67] G. A. Lalazissis, J. Konig, and P. Ring, Phys. Rev. **C55**, 540 (1997).
[68] G. A. Lalazissis, S. Raman, and P. Ring, At. Data Nucl. Data Tables **71**, 1 (1999).
[69] B. G. Todd-Rutel and J. Piekarewicz, Phys. Rev. Lett **95**, 122501 (2005).
[70] F. J. Fattoyev, C. J. Horowitz, J. Piekarewicz, and G. Shen, Phys. Rev. **C82**, 055803 (2010).
[71] A. W. Steiner, J. M. Lattimer, and E. F. Brown, Astrophys. J. **722**, 33 (2010).
[72] M. Wang, G. Audi, A. H. Wapstra, F. G. Kondev, M. MacCormick, X. Xu, and B. Pfeiffer, Chinese Phys. C **36**, 1603 (2012).